Anisotropic effects in highly scattering media

Jenni Heino*
Laboratory of Biomedical Engineering, Helsinki University of Technology, P. O. Box 2200, 02015 HUT, Finland

Simon Arridge† and Jan Sikora‡
Department of Computer Science, University College London, Gower Street, London WC1E 6BT, United Kingdom

Erkki Somersalo§
Laboratory of Mathematics, Helsinki University of Technology, P. O. Box 1100, 02015 HUT, Finland
(Received 5 May 2003; published 18 September 2003)

In this paper, we study anisotropic scattering and light propagation models applicable to diffuse optical tomography. We propose a model for anisotropic scattering in the radiative transfer framework and derive the corresponding anisotropic diffusion model. To verify the anisotropic diffusion model, we consider the case of a simple anisotropic scattering model also presentable within the diffusion approximation. For numerical computations, we present a three-dimensional (3D) anisotropic Monte Carlo model and 2D finite element and boundary element solutions of the anisotropic diffusion model, and compare the results of the simulations.

DOI: 10.1103/PhysRevE.68.031908 PACS number(s): 87.64.Cc, 78.20.Bh

I. INTRODUCTION

Optical tomography [1] is a relatively new and developing noninvasive medical imaging modality. In optical tomography, measurements of scattered and transmitted near-infrared light on the surface of the body are used for reconstruction of the internal distribution of optical properties inside the body. The strong scattering of near-infrared light in most human tissues renders the related inverse problem of the estimation of the optical properties a highly involved one, requiring advanced modeling and reconstruction techniques. One point in theoretical developments toward a more succesful estimation is the investigation of light propagation models that can be used to predict boundary measurements more faithfully.

Several human tissue types have properties that depend not only on location but also on direction. One example is the white matter of the brain, where the orientation of the axon fiber bundles gives rise to directionally dependent diffusion properties of water. Another example of structural anisotropy is the muscle fibers. Anisotropic light propagation has been measured in chicken breast tissue [2] and human skin [3] and dentin [4]; hence there is good reason to believe that such structural anisotropy is seen in the optical regime. Proper modeling and understanding of the effects of anisotropy may provide valuable information for imaging and reconstruction in optical tomography.

A commonly used model for light propagation in optical tomography is the isotropic diffusion equation, which can be derived from the equation of radiative transfer under certain conditions often met in biological tissue. To handle anisotropic media, in [5], an anisotropic form of the diffusion equation was derived and used to investigate the effects of anisotropy on image reconstruction. Another diffusionlike approach to model anisotropic light propagation presented in [6] was based on the continuous-time random walk model.

In this paper, we consider in more detail an anisotropic scattering and light propagation model based on the radiative transfer equation. We present a possible model for anisotropic scattering applicable in the radiative transfer framework and then derive the corresponding anisotropic diffusion approximation. In our numerical experiments, the anisotropic diffusion equation is solved using both finite element and boundary element methods, and the results compared to a Monte Carlo simulation based on the radiative transfer equation and the anisotropic scattering model.

II. SCATTERING AND LIGHT PROPAGATION MODELS

A. Radiative transfer equation

In optical tomography light propagation is generally modeled using the radiative transfer equation (RTE) [7], also known as the Boltzmann equation. For time dependent problems, this is written

$$\left(\frac{1}{c}\frac{\partial}{\partial t}+\hat{\boldsymbol{s}}\cdot\nabla+\mu_{\mathrm{a}}(\boldsymbol{r})+\mu_{\mathrm{s}}(\boldsymbol{r})\right)\phi(\boldsymbol{r},\hat{\boldsymbol{s}},t) = \mu_{\mathrm{s}}(\boldsymbol{r})\int_{S^2}\Theta(\hat{\boldsymbol{s}},\hat{\boldsymbol{s}}',\boldsymbol{r})\,\phi(\boldsymbol{r},\hat{\boldsymbol{s}}',t)\,\mathrm{d}\hat{\boldsymbol{s}}'+q(\boldsymbol{r},\hat{\boldsymbol{s}},t), \tag{1}$$

where μ_{a} and μ_{s} are the absorption and scattering coefficients, respectively, $\phi(\boldsymbol{r},\hat{\boldsymbol{s}},t)$ is the radiance at position $\boldsymbol{r}$ with direction of propagation $\hat{\boldsymbol{s}}$, c is the speed of light, q denotes the source term, and Θ is the *phase function* for the scattering. In operator form we write this as

$$\frac{1}{c}\frac{\partial\phi}{\partial t}+\mathcal{T}(\mu_{\mathrm{a}},\mu_{\mathrm{s}})[\phi]=\mathcal{S}(\mu_{\mathrm{s}})[\phi]+q. \tag{2}$$

The scattering coefficient represents the probability density per unit volume of a scattering event. The phase function

*Email address: Jenni.Heino@hut.fi
†Email address: S.Arridge@cs.ucl.ac.uk
‡Email address: J.Sikora@cs.ucl.ac.uk
§Email address: Erkki.Somersalo@hut.fi

or the differential scattering kernel Θ represents the probability density of a particle scattering from direction $\hat{\boldsymbol{s}}'$ into $\hat{\boldsymbol{s}}$. In isotropic media, it is assumed to be stationary—i.e., dependent only on the angle between incoming direction $\hat{\boldsymbol{s}}'$ and outgoing direction $\hat{\boldsymbol{s}}$. Then we can write

$$\Theta_{\mathrm{iso}}(\hat{\boldsymbol{s}},\hat{\boldsymbol{s}}',\boldsymbol{r}) \equiv \Theta(\hat{\boldsymbol{s}}\cdot\hat{\boldsymbol{s}}',\boldsymbol{r}).$$

In anisotropic media this is no longer the case. The question then arises as to the appropriate form for $\Theta(\hat{\boldsymbol{s}},\hat{\boldsymbol{s}}',\boldsymbol{r})$.

B. Scattering phase function

1. Properties of the scattering phase function

The following properties of the phase function are apparent on physical grounds: (1) the probability density of scattering cannot be negative,

$$\Theta(\hat{\boldsymbol{s}},\hat{\boldsymbol{s}}') \geqslant 0 \quad \forall\ \hat{\boldsymbol{s}},\hat{\boldsymbol{s}}' \in S^2, \tag{3}$$

(2) there is reciprocity of light propagation,

$$\Theta(\hat{\boldsymbol{s}},\hat{\boldsymbol{s}}') = \Theta(-\hat{\boldsymbol{s}}',-\hat{\boldsymbol{s}}), \tag{4}$$

and (3) the probability of scattering over the sphere is unity regardless of the incoming radiation direction,

$$\int_{S^2} \Theta(\hat{\boldsymbol{s}},\hat{\boldsymbol{s}}')\,\mathrm{d}\hat{\boldsymbol{s}} = 1 \qquad \forall\ \hat{\boldsymbol{s}}' \in S^2. \tag{5}$$

2. Isotropic scattering

In the isotropic case a convenient model for Θ_{iso} is the *Henyey-Greenstein* function [8]

$$H_3(\hat{\boldsymbol{s}}\cdot\hat{\boldsymbol{s}}';g) = \frac{1}{4\pi}\frac{1-g^2}{(1+g^2-2g\hat{\boldsymbol{s}}\cdot\hat{\boldsymbol{s}}')^{3/2}}, \tag{6}$$

which has the useful property that its Legendre expansion is given by powers of the parameter g:

$$\Theta_l := \int_{S^2} P_l(\tau)\Theta(\tau)\,\mathrm{d}\hat{\boldsymbol{s}}' = g^l, \tag{7}$$

and (using an addition theorem for Legendre polynomials) we have the expansion

$$H_3(\hat{\boldsymbol{s}}\cdot\hat{\boldsymbol{s}}';g) = \sum_{l}^{\infty}\sum_{m=-l}^{l} g^l \overline{Y}_{l,m}(\hat{\boldsymbol{s}}')Y_{l,m}(\hat{\boldsymbol{s}}), \tag{8}$$

where $Y_{l,m}$ are the spherical harmonics. Here $g \in (-1,1)$ serves as a measure of the forward scattering bias, with $g = 0$ corresponding to uniform scattering.[1]

The two-dimensional analog of this function is

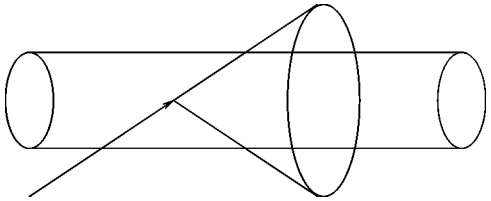

FIG. 1. A schematic representation of anisotropic scattering. The main direction of anisotropy is parallel to the axis of the cylinder. The component of light parallel to the axis is preserved in the scattering, whereas the perpendicular component is randomly oriented, forming a cone shape for the possible scattering directions.

$$H_2(\varphi,\varphi';g) = \frac{1}{2}\frac{1-g^2}{1+g^2-2g\cos(\varphi-\varphi')}. \tag{9}$$

Note that H_2 is not simply the integral over the azimuthal direction of H_3. H_2 has a Fourier series representation [rather than the Legendre series of Eq. (7)]:

$$H_2(\varphi,\varphi') = \frac{1}{2\pi} + \frac{1}{\pi}\sum_{n=1}^{\infty} g^n \cos[n(\varphi-\varphi')]. \tag{10}$$

3. Anisotropic scattering

As a model of the anisotropic case consider the case of an infinite cylinder oriented along the z axis [3]. If we assume that the direction of scattering is unchanged in z we have the model

$$\begin{aligned}\Theta_{\mathrm{aniso}}(\hat{\boldsymbol{s}},\hat{\boldsymbol{s}}') &= \Theta(\vartheta,\vartheta',\varphi,\varphi';g_\perp)\\ &= \delta(\cos\vartheta - \cos\vartheta')H_2(\varphi,\varphi';g_\perp).\end{aligned} \tag{11}$$

This has the requisite properties (3)–(5). We might also choose a proper (symmetric) function $Z(\vartheta,\vartheta')$ such that

$$\int_0^{\pi} Z(\vartheta,\vartheta')\sin\vartheta\,\mathrm{d}\vartheta = 1$$

in place of the δ function in Eq. (11). Figure 1 illustrates this model for anisotropic scattering.

By writing the spherical harmonics

$$Y_{l,m}(\vartheta,\varphi) = P_l^m(x)\mathrm{e}^{\mathrm{i}m\varphi}, \quad x = \cos\vartheta,$$

where $P_l^m(x)$ are the associated normalized Legendre polynomials, it is easily verified that

$$\int_{S^2} \Theta_{\mathrm{aniso}}(\hat{\boldsymbol{s}},\hat{\boldsymbol{s}}')Y_{l,m}(\hat{\boldsymbol{s}}')\,\mathrm{d}\hat{\boldsymbol{s}}' = g_\perp^{|m|}Y_{l,m}(\hat{\boldsymbol{s}})$$

and

$$\int_{S^2} \Theta_{\mathrm{aniso}}(\hat{\boldsymbol{s}},\hat{\boldsymbol{s}}')\overline{Y}_{l,m}(\hat{\boldsymbol{s}})\,\mathrm{d}\hat{\boldsymbol{s}} = g_\perp^{|m|}\overline{Y}_{l,m}(\hat{\boldsymbol{s}}'),$$

so we have the biharmonic expansion

[1]The factor g is frequently termed the *anisotropy factor* when considering the directionally independent scattering case. However, we will use the term *bias factor* to avoid confusion.

$$\Theta_{\text{aniso}}(\hat{\boldsymbol{s}},\hat{\boldsymbol{s}}')=\sum_{l}^{\infty}\sum_{m=-l}^{l} g_{\perp}^{|m|}\overline{Y}_{l,m}(\hat{\boldsymbol{s}}')Y_{l,m}(\hat{\boldsymbol{s}}). \tag{12}$$

C. Diffusion approximation

1. Isotropic diffusion approximation

A standard approximation method for the RTE is to expand the radiance ϕ and the source term q in Eq. (1) into spherical harmonics and truncate the series. The spherical harmonics expansions can be written as

$$\phi(\boldsymbol{r},\hat{\boldsymbol{s}})=\sum_{l}^{\infty}\sum_{m=-l}^{l}\phi_{lm}(\boldsymbol{r})Y_{l,m}(\hat{\boldsymbol{s}}), \tag{13}$$

$$q(\boldsymbol{r},\hat{\boldsymbol{s}})=\sum_{l}^{\infty}\sum_{m=-l}^{l}q_{lm}(\boldsymbol{r})Y_{l,m}(\hat{\boldsymbol{s}}). \tag{14}$$

Inserting the isotropic scattering phase function (8) in the operator $\mathcal{S}$ in Eq. (2) yields the expansion

$$\mathcal{S}(\mu_{\text{s}})[\phi]=\mu_{\text{s}}\sum_{l}^{\infty}\sum_{m=-l}^{l} g^{l}\phi_{lm}(\boldsymbol{r})Y_{l,m}(\hat{\boldsymbol{s}}). \tag{15}$$

For the diffusion model the spherical harmonics expansion is taken only up to first order. For ϕ, truncating the series (13) at $l=1$ yields after some manipulation

$$\phi(\boldsymbol{r},\hat{\boldsymbol{s}},t)=\frac{1}{4\pi}\int_{S^2}\phi(\boldsymbol{r},\hat{\boldsymbol{s}}',t)\mathrm{d}\hat{\boldsymbol{s}}'+\frac{3}{4\pi}\hat{\boldsymbol{s}}\cdot\int_{S^2}\hat{\boldsymbol{s}}'\,\phi(\boldsymbol{r},\hat{\boldsymbol{s}}',t)\mathrm{d}\hat{\boldsymbol{s}}'. \tag{16}$$

Similarly, the first order approximations for Eqs. (14) and (15) are obtained by truncating the series at $l=1$.

Next, introducing some standard notation, the *photon density* is defined as

$$\Phi(\boldsymbol{r},t)=\int_{S^2}\phi(\boldsymbol{r},\hat{\boldsymbol{s}},t)\mathrm{d}\hat{\boldsymbol{s}} \tag{17}$$

and the *photon current* as

$$\boldsymbol{J}(\boldsymbol{r},t)=\int_{S^2}\hat{\boldsymbol{s}}\phi(\boldsymbol{r},\hat{\boldsymbol{s}},t)\mathrm{d}\hat{\boldsymbol{s}}, \tag{18}$$

while the corresponding source terms are the *isotropic* and *dipole* terms

$$Q_0(\boldsymbol{r},t)=\int_{S^2}q(\boldsymbol{r},\hat{\boldsymbol{s}},t)\mathrm{d}\hat{\boldsymbol{s}}, \tag{19}$$

$$\boldsymbol{Q}_1(\boldsymbol{r},t)=\int_{S^2}\hat{\boldsymbol{s}}q(\boldsymbol{r},\hat{\boldsymbol{s}},t)\mathrm{d}\hat{\boldsymbol{s}}. \tag{20}$$

By integrating the RTE (1) and the RTE multiplied by $\hat{\boldsymbol{s}}$ over S^2 and using the first order approximations for the radiance ϕ and the source term q and the notation in Eqs. (17)– (20), we arrive after some lengthy calculations at a set of coupled equations:

$$\left(\frac{1}{c}\frac{\partial}{\partial t}+\mu_{\text{a}}(\boldsymbol{r})\right)\Phi(\boldsymbol{r},t)+\nabla\cdot\boldsymbol{J}(\boldsymbol{r},t)=Q_0(\boldsymbol{r},t), \tag{21}$$

$$\left(\frac{1}{c}\frac{\partial}{\partial t}+\mu_{\text{a}}(\boldsymbol{r})+(1-g)\mu_{\text{s}}(\boldsymbol{r})\right)\boldsymbol{J}(\boldsymbol{r},t)+\frac{1}{3}\nabla\Phi(\boldsymbol{r},t)=\boldsymbol{Q}_1(\boldsymbol{r},t). \tag{22}$$

Equations (21) and (22) are termed the $P1$ approximation. To get a single second order partial differential equation we make two more simplifications, assuming that $\partial\boldsymbol{J}/\partial t$ is negligible in Eq. (22) (or, alternatively, proportional to $\boldsymbol{J}$) and that the anisotropic source terms are zero, i.e., $\boldsymbol{Q}_1=\boldsymbol{0}$. Then

$$\boldsymbol{J}=-D\nabla\Phi, \tag{23}$$

where the *diffusion coefficient* is defined by

$$D=\frac{1}{3(\mu_{\text{a}}+\mu_{\text{s}}')} \tag{24}$$

and $\mu_{\text{s}}'=(1-g)\mu_{\text{s}}$ is the *reduced scattering coefficient*. Finally, we arrive at the diffusion equation as normally used in optical tomography:

$$\frac{1}{c}\frac{\partial}{\partial t}\Phi(\boldsymbol{r},t)-\nabla\cdot D(\boldsymbol{r})\nabla\Phi(\boldsymbol{r},t)+\mu_{\text{a}}(\boldsymbol{r})\Phi(\boldsymbol{r},t)=Q_0(\boldsymbol{r},t). \tag{25}$$

2. Anisotropic diffusion approximation

Utilizing Eq. (12) we have

$$\mathcal{S}(\mu_{\text{s}})[\phi]=\mu_{\text{s}}\sum_{l}^{\infty}\sum_{m=-l}^{l} g_{\perp}^{|m|}\phi_{lm}(\boldsymbol{r})Y_{l,m}(\hat{\boldsymbol{s}}).$$

The diffusion equation results from the termination of this series at $l=1$. Employing the standard derivation, we get the anisotropic diffusion equation

$$\frac{1}{c}\frac{\partial}{\partial t}\Phi(\boldsymbol{r},t)-\nabla\cdot\mathsf{D}(\boldsymbol{r})\nabla\Phi(\boldsymbol{r},t)+\mu_{\text{a}}(\boldsymbol{r})\Phi(\boldsymbol{r},t)=Q_0(\boldsymbol{r},t), \tag{26}$$

where the *diffusion tensor* is given by

$$\mathsf{D}=\frac{1}{3}[(\mu_{\text{a}}+\mu_{\text{s}})\mathsf{I}-\mu_{\text{s}}\mathsf{S}_1]^{-1}$$

with

$$\mathsf{I}=\begin{pmatrix}1&0&0\\0&1&0\\0&0&1\end{pmatrix}$$

and

$$\mathsf{S}_1=\begin{pmatrix}g_{\perp}&0&0\\0&g_{\perp}&0\\0&0&1\end{pmatrix}.$$

We can also consider the case where we imagine a mixture of oriented fibers with density $f\mu_s$ and isotropic scatterers with density $(1-f)\mu_s$ (where f is a fraction $0 \leqslant f \leqslant 1$).[2] Let the latter have bias g_0. The resulting diffusion tensor will be

$$\mathsf{S}_1 = \begin{pmatrix} fg_\perp + (1-f)g_0 & 0 & 0 \\ 0 & fg_\perp + (1-f)g_0 & 0 \\ 0 & 0 & f + (1-f)g_0 \end{pmatrix}.$$

To obtain the case where the fibres are oriented along another direction $\hat{\boldsymbol{s}}_1 = (\zeta, \xi)$ we only need to rotate the tensor:

$$\mathsf{D} \rightarrow \mathsf{R}\mathsf{D}\,\mathsf{R}^{\mathrm{T}}.$$

3. Frequency domain

A common experimental method is to modulate the intensity of the light source with a radio-frequency signal. For a source function modulated with angular frequency ω the diffusion equation can be written in the frequency domain by taking a Fourier transform of the time domain diffusion equation (26):

$$-\frac{i\omega}{c}\Phi(\boldsymbol{r};\omega) - \nabla \cdot \mathsf{D}(\boldsymbol{r})\nabla\Phi(\boldsymbol{r};\omega) + \mu_a(\boldsymbol{r})\Phi(\boldsymbol{r};\omega) = Q_0(\boldsymbol{r};\omega), \tag{27}$$

where $\Phi(\boldsymbol{r};\omega)$ is the complex density arising from the intensity modulated part $Q_0(\boldsymbol{r};\omega)$ of the source term.

4. Source and boundary conditions

In this work, we use the so called collimated source approximation [9], where the light source is modeled with a collimated pencil beam perpendicular to the surface. In this approximation, we write the source term as a point source below the surface: $Q_0(\boldsymbol{r};\omega) = Q_0(\omega)\,\delta(\boldsymbol{r}-\boldsymbol{r}_s)$, where $\boldsymbol{r}_s$ is the source position. For the boundary condition, we assume that the inward directed current at each point on the boundary is zero. Within the diffusion approximation, this assumption leads to a so-called Robin boundary condition:

$$\Phi + 2\hat{\boldsymbol{n}} \cdot \mathsf{D}\nabla\Phi = 0, \tag{28}$$

where $\hat{n}$ is the outward unit vector normal to the surface and the refractive index is assumed to be 1. The boundary data consist of measured outward flux $\Gamma_{\mathrm{out}} = -\hat{\boldsymbol{n}} \cdot \mathsf{D}\nabla\Phi$ at points $\boldsymbol{r}_m$, the optode locations, on the boundary $\partial\Omega$. Using the boundary condition (28), the outward flux within the diffusion approximation is simply $\Gamma_{\mathrm{out}}(\boldsymbol{r}_m) = \frac{1}{2}\Phi(\boldsymbol{r}_m)$.

[2]Technically we might have to consider more carefully the meaning of the scattering coefficient for fibers since it may be directionally dependent too. See [3] for a fuller discussion.

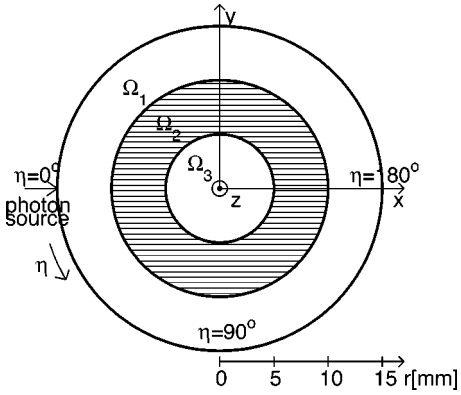

FIG. 2. Geometry used in the simulations.

III. NUMERICAL EXPERIMENTS

In our numerical experiments, we compare the results from a Monte Carlo simulation based on the radiative transfer model and from the finite element (FEM) and boundary element (BEM) methods based on the diffusion model. The Monte Carlo simulations were performed in a three-dimensional (3D) cylinder oriented parallel to the z axis, with a cross section as depicted in Fig. 2, and the FEM and BEM simulations in an equivalent 2D circle. The photons are incident on the domain at the position $\eta = 0°$ on the boundary, and measured all around the boundary of the domain.

The outer- and innermost layers Ω_1 and Ω_3 in the circle are isotropic, and the middle layer Ω_2 is anisotropic with the direction of anisotropy parallel to the x axis as illustrated by the horizontal stripes. In the isotropic layers the scattering is assumed to be uniform, i.e., the forward scattering bias is assumed to have a value $g = 0$. The anisotropic layer is assumed to consist of a mixture of oriented fibers (density f, direction of scattering unchanged) and isotropic scatterers [density $(1-f)$, bias $g_0 = 0$]. The parameter values used in the simulations are listed in Table I.

A. Monte Carlo simulation

In the Monte Carlo simulation, the propagation of a photon or a photon package is simulated through the medium. This is done by following the photon's path and sequentially modeling each event the photon undergoes during its travel in the medium.

The anisotropic Monte Carlo simulation code used here was based on an isotropic code [10] and proceeds in the following way. First, a photon package is launched into the

TABLE I. The parameter values used for numerical calculations.

	Isotropic media	Anisotropic media
μ_a	0.1 mm^{-1}	0.1 mm^{-1}
μ_s	10 mm^{-1}	10 mm^{-1}
g	0	
f		0.9
g_0		0
$g_\perp$		0

domain perpendicular to the boundary at the source position. Subsequently, at each step, part $[1-\exp(-\mu_a l)]$ of the package is absorbed, where l is the propagation length. The propagation length is drawn from an exponential distribution with mean proportional to the scattering coefficient. In the isotropic medium, the new propagation direction is drawn from a uniform probability distribution in solid angle. In the anisotropic medium, an anisotropic scattering event takes place with probability f; otherwise an isotropic scattering event is modeled as in the isotropic layers. In the anisotropic scattering, the x component of the direction vector is preserved and only the yz components are redrawn from a uniform distribution.

In the Monte Carlo simulation, the source was assumed to be located at a single point $(-15,0,0)$ on the boundary. However, to compare the results with the 2D diffusion computations, the detectors were modeled as line detectors parallel to the axis of the cylinder on the boundary of the cylinder, and the detected light was recorded as a function of the boundary position angle η only. The phase shift and the complex intensity of the package on the boundary were calculated based on the path length of the package. The aperture of the cylinder in the z direction was 5 mm, and photons exiting from the ends of the cylinder were recorded as lost.

B. Finite element method

For implementing the finite element method, we use the so-called Galerkin formulation. First, we write the variational formulation of the diffusion equation (27). By multiplying Eq. (27) by a test function ψ, integrating by parts over Ω, and using the Gauss and Green's theorems, we arrive at the weak formulation of the diffusion equation: Find Φ such that

$$\int_\Omega \nabla\psi\cdot \mathsf{D}\nabla\Phi\, d\mathbf{r} + \int_\Omega \left(\mu_a - \frac{i\omega}{c}\right)\psi\Phi\, d\mathbf{r} + \int_{\partial\Omega}\frac{1}{2}\psi\Phi\, dS = Q_0\psi(\mathbf{r}_s) \tag{29}$$

$\forall\ \psi\in H^1(\Omega)$, where $H^1(\Omega)$ is a predefined function space (Sobolev space) for the test functions. In Eq. (29), the Robin boundary condition (28) and the collimated source condition have been taken into account.

In the finite element approximation, the domain Ω is divided into finite elements and the solution is approximated by nodal-based basis functions,

$$\Phi(\mathbf{r})\approx\sum_{j=1}^{N_n}\alpha_j\psi_j(\mathbf{r}), \tag{30}$$

where N_n is the number of nodes in the finite element mesh. By choosing the test function ψ in Eq. (29) to be one of the basis functions, we arrive at the matrix equation $A\alpha=\beta$, where A is the $N_n\times N_n$ symmetric matrix with entries

$$A_{j,\ell} = \int_\Omega \nabla\psi_j\cdot\mathsf{D}\nabla\psi_\ell\, d\mathbf{r} + \int_\Omega\left(\mu_a-\frac{i\omega}{c}\right)\psi_j\psi_\ell\, d\mathbf{r} + \int_{\partial\Omega}\frac{1}{2}\psi_j\psi_\ell\, dS, \tag{31}$$

and β is an N_n–vector $\beta_j=Q_0\psi_j(\mathbf{r}_s)$.

In two dimensions, we write the diffusion tensor D as

$$\mathsf{D}(\mathbf{r})=\mathsf{R}(\mathbf{r})\,\mathrm{diag}[\lambda_1(\mathbf{r}),\lambda_2(\mathbf{r})]\mathsf{R}(\mathbf{r})^T, \tag{32}$$

where $\mathsf{R}(\mathbf{r})$ is a 2×2 real orthogonal matrix, and

$$\lambda_j(\mathbf{r})=\frac{1}{3\{\mu_a(\mathbf{r})+[1-b_j(\mathbf{r})]\mu_s(\mathbf{r})\}},\qquad j=1,2. \tag{33}$$

In the isotropic case we have simply $b_1^{\mathrm{iso}}=b_2^{\mathrm{iso}}=g=0$. In the anisotropic case considered here, we have $b_1^{\mathrm{aniso}}=f+(1-f)g_0=f$ and $b_2^{\mathrm{aniso}}=fg_\perp+(1-f)g_0=0$.

The representation (32) can also be interpreted as an eigenvalue decomposition of the diffusion tensor. The eigenvalues λ_j, $j=1,2$, present the strength of the anisotropy, and the direction of anisotropy is confined in the matrix R.

C. Boundary element method

In the BEM formulation, we assume that the body Ω is divided into nested subdomains Ω_i, $1\leqslant i\leqslant n$, where Ω_1 is the outermost one. Each subdomain is characterized by constant material parameters. Let D_i and $\mu_{a,i}$ denote the diffusion tensor and absorption coefficient in Ω_i. We denote

$$k_i=(\mu_{a,i}-i\omega/c)^{1/2},$$

where the branch of the square root is chosen so that $\mathrm{Re}\ k_i>0$. The Green's functions G_i corresponding to each subdomain are defined as solutions of the equations

$$\nabla\cdot\mathsf{D}_i\nabla G_i(\mathbf{r},\mathbf{r}')-k_i^2G_i(\mathbf{r},\mathbf{r}')=-\delta(\mathbf{r}-\mathbf{r}')\quad\text{in}\quad\mathbb{R}^2$$

with the asymptotics

$$G_i(\mathbf{r},\mathbf{r}')|_{|\mathbf{r}|\to\infty}=0.$$

By a change of variables $\mathbf{r}\to\tilde{\mathbf{r}}=\mathsf{D}_i^{-1/2}\mathbf{r}$, one can verify that G_i can be written as

$$G_i(\mathbf{r},\mathbf{r}')=\frac{i}{4|\mathsf{D}_i|}H_0^{(1)}(ik_i|\mathbf{r}-\mathbf{r}'|_i)=\frac{1}{2\pi|\mathsf{D}_i|}K_0(k_i|\mathbf{r}-\mathbf{r}'|_i),$$

where K_0 is the modified Bessel function of the second kind, $|\mathsf{D}_i|=\det(\mathsf{D}_i)$, and the shorthand notation

$$|\mathbf{r}-\mathbf{r}'|_i=[(\mathbf{r}-\mathbf{r}')\mathsf{D}_i^{-1}(\mathbf{r}-\mathbf{r}')]^{1/2}$$

was used.

Let Φ_i denote the restriction of Φ to the subdomain Ω_i,

$$\nabla\cdot\mathsf{D}_i\nabla\Phi_i(\mathbf{r})-k_i^2\Phi_i(\mathbf{r})=-Q_i(\mathbf{r})\,\text{in}\,\Omega_i,$$

where the source term $Q_i = Q_0 \delta_{i,1}$ is nonzero only for $i=1$. If Γ_i is the interface between Ω_i and Ω_{i+1}, $1 \leqslant i \leqslant n-1$, the subsolutions Φ_i must satisfy the interface conditions

$$\Phi_i|_{\Gamma_i} = \Phi_{i+1}|_{\Gamma_i} = \nu_i,$$

$$\partial_i \Phi_i|_{\Gamma_i} = \partial_{i+1}\Phi_{i+1}|_{\Gamma_i} = \rho_i, \quad 1 \leqslant i \leqslant n-1,$$

where we used the abbreviated notation

$$\partial_i = \hat{n} \cdot \mathsf{D}_i \nabla$$

for the conormal derivatives. Here, $\hat{\boldsymbol{n}}$ denotes the exterior unit vector normal to the surface Γ_i or Γ_{i-1}. On the exterior surface of the body, denoted by Γ_0, we have the Robin boundary condition [cf. Eq. (28)]

$$\nu_0 + 2\rho_0 = 0, \tag{34}$$

where

$$\nu_0 = \Phi_1|_{\Gamma_0}, \quad \rho_0 = \partial_1 \Phi_1|_{\Gamma_0}.$$

By applying a second Green's theorem in Ω_i, we obtain the representation

$$\Phi_i(\mathbf{r}) = \left(\int_{\Gamma_{i-1}} - \int_{\Gamma_i} \right) [G_i(\mathbf{r},\mathbf{r}')\partial_i \Phi_i(\mathbf{r}') - \Phi_i(\mathbf{r}')\partial_i G_i(\mathbf{r},\mathbf{r}')] dS(\mathbf{r}') + q_i(\mathbf{r}), \tag{35}$$

where it is understood that $\Gamma_n = \varnothing$ and the source term q_i is

$$q_i(\mathbf{r}) = \int_{\Omega_i} G_i(\mathbf{r},\mathbf{r}') Q_i(\mathbf{r}') d\mathbf{r}'.$$

To obtain the boundary integral equations, let $\mathbf{r}$ approach first the outer boundary Γ_{i-1}. By using the properties of the layer potential operators [11] and the notation introduced earlier, we obtain

$$C^+_{i-1}(\mathbf{r})\nu_{i-1}(\mathbf{r}) + \int_{\Gamma_{i-1}} [\partial_i G_i(\mathbf{r},\mathbf{r}')\nu_{i-1}(\mathbf{r}') - G_i(\mathbf{r},\mathbf{r}')\rho_{i-1}(\mathbf{r}')] dS(\mathbf{r}') - \int_{\Gamma_i} [\partial_i G_i(\mathbf{r},\mathbf{r}')\nu_i(\mathbf{r}') - G_i(\mathbf{r},\mathbf{r}')\rho_i(\mathbf{r}')] dS(\mathbf{r}') = q_i(\mathbf{r}), \quad 1 \leqslant i \leqslant n. \tag{36}$$

Observe that above the first integral is singular while the second one has a continuous kernel. Similarly, letting the variable $\mathbf{r}$ approach the inner interface Γ_i, we arrive at the equation

$$C^-_{i-1}(\mathbf{r})\nu_i(\mathbf{r}) - \int_{\Gamma_i} [\partial_i G_i(\mathbf{r},\mathbf{r}')\nu_i(\mathbf{r}') - G_i(\mathbf{r},\mathbf{r}')\rho_i(\mathbf{r}')] dS(\mathbf{r}') + \int_{\Gamma_{i-1}} [\partial_i G_i(\mathbf{r},\mathbf{r}')\nu_{i-1}(\mathbf{r}') - G_i(\mathbf{r},\mathbf{r}')\rho_{i-1}(\mathbf{r}')] dS(\mathbf{r}') = q_i(\mathbf{r}), \quad 1 \leqslant i \leqslant n-1. \tag{37}$$

The extra function $C^{\pm}_i(\mathbf{r})$, arises due to singularities on the boundary. However, as shown in [12,13], this term does not need to be calculated explicitly and can be obtained indirectly by utilizing some simple physical considerations. In particular, we have $C^+_i(\mathbf{r}) = C^-_i(\mathbf{r}) = \frac{1}{2}$ when the observation point lies on a smooth surface, which is the case considered here.

Using Eq. (34) to trivially eliminate one unknown, Eqs. (36) and (37) constitute a system of $2n-1$ coupled integral equations for the $2n-1$ unknown functions $\nu_0, \ldots, \nu_{n-1}, \rho_1, \ldots, \rho_{n-1}$. Solving for these functions, the representation formula (35) yields the field Φ.

Similar to the FEM, the BEM equations are solved by discretizing each surface Γ_i into P_i elements with N_i vertices, but here both ν_i and ρ_i are approximated by the nodal basis functions (restricted to Γ_i)

$$\nu_i(\mathbf{r}) \approx \sum_{j=1}^{N_i} \nu_{i,j}\psi_{i,j}(\mathbf{r}), \quad \rho_i(\mathbf{r}) \approx \sum_{j=1}^{N_i} \rho_{i,j}\psi_{i,j}(\mathbf{r}). \tag{38}$$

The result is a system of dense unsymmetric block matrices which are solved using a preconditioned GMRES solver.

D. Connection between 2D and 3D models

Consider the diffusion equation (27) and the boundary condition (28) in the case that the body $\Omega \subset \mathbb{R}^3$ is a long cylinder. We assume that it is long enough to justify an infinitely long cylinder as a model, i.e., $\Omega = U \times \mathbb{R}$, where $U \subset \mathbb{R}^2$ is the horizontal intersection of the cylinder. Let us assume that the source $Q_0 = Q_0(x,y,z)$ is restricted to a finite section of the cylinder, i.e., $Q_0(x,y,z) = 0$ for $|z|$ large. Then the field Φ satisfies

$$\Phi|_{|z|\to\infty} = 0, \quad \nabla\Phi|_{|z|\to\infty} = 0. \tag{39}$$

Assume further that $\mathsf{D} = \mathsf{D}(x,y)$ and $\mu_a = \mu_a(x,y)$, $(x,y) \in D$, i.e., the material parameters are constants along the cylinder. Let us factor the tensor D as

$$\mathsf{D} = \begin{bmatrix} \mathsf{D}_\perp & \boldsymbol{w} \\ \boldsymbol{w}^{\mathrm{T}} & \mathsf{D}_{33} \end{bmatrix}, \quad \mathsf{D}_\perp \in \mathbb{R}^{2\times 2}, \quad \boldsymbol{w} \in \mathbb{R}^{2\times 1}.$$

Further, by writing

$$\nabla\Phi = (\partial_x \Phi \mathbf{e}_1 + \partial_y \Phi \mathbf{e}_2) + \partial_z \Phi \mathbf{e}_3 = \nabla_\perp \Phi + \partial_z \Phi \mathbf{e}_3,$$

we have

$$\mathsf{D}\nabla\Phi = \mathsf{D}_\perp \nabla_\perp \Phi + \boldsymbol{w}\partial_z\Phi + (\boldsymbol{w}\cdot\nabla_\perp\Phi + \mathsf{D}_{33}\partial_z\Phi)\mathbf{e}_3,$$

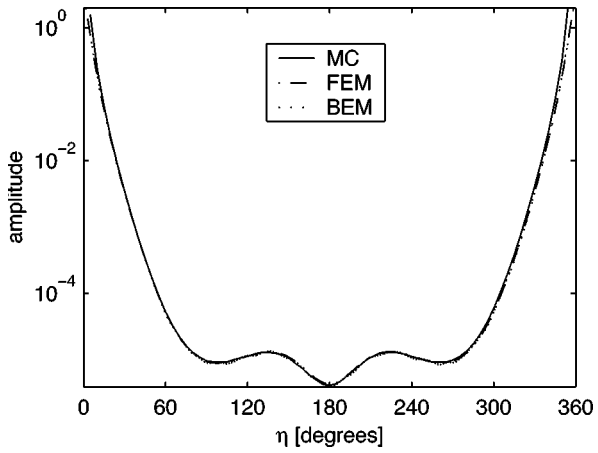

FIG. 3. Amplitude on the boundary in the anisotropic model using Monte Carlo simulation, FEM, and BEM. The MC and BEM curves have been normalized using the FEM/MC and FEM/BEM relations, respectively, at $\eta = 45°$.

and further, by using the fact that $\boldsymbol{w}$ is independent of z,

$$\nabla(\mathsf{D}\nabla\Phi) = \nabla_\perp \cdot \mathsf{D}_\perp \nabla_\perp \Phi + \partial_z u, \tag{40}$$

where the function u is

$$u = \nabla_\perp \cdot (\boldsymbol{w}\Phi) + \boldsymbol{w} \cdot \nabla_\perp \Phi + \mathsf{D}_{33}\partial_z \Phi$$
$$= (\nabla_\perp \cdot \boldsymbol{w})\Phi + 2\boldsymbol{w} \cdot \nabla_\perp \Phi + \kappa_{33}\partial_z \Phi.$$

Let us define the vertically averaged field,

$$\Phi_{\mathrm{av}}(x,y) = \int_{-\infty}^{\infty} \Phi(x,y,z)dz.$$

By integrating Eq. (27) over the vertical axis and using the decomposition (40), we may argue first that

$$\int_{-\infty}^{\infty} \nabla(\mathsf{D}\nabla\Phi)dz = \nabla_\perp \cdot \mathsf{D}_\perp \nabla_\perp \Phi_{\mathrm{av}} + \Big|_{z=-\infty}^{z=\infty} u = \nabla_\perp \cdot \mathsf{D}_\perp \nabla_\perp \Phi_{\mathrm{av}},$$

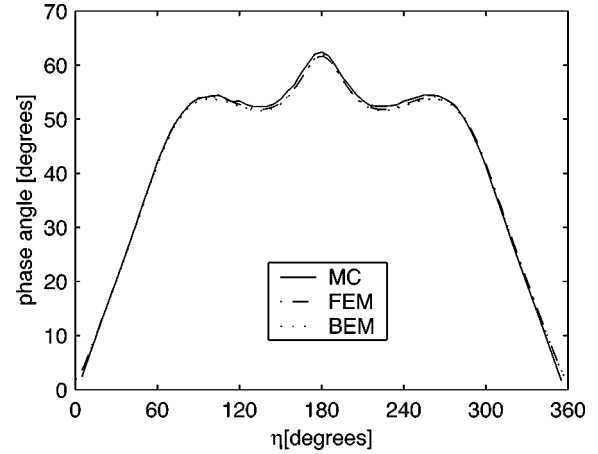

FIG. 4. Phase angle on the boundary in the anisotropic model using Monte Carlo simulation, FEM, and BEM.

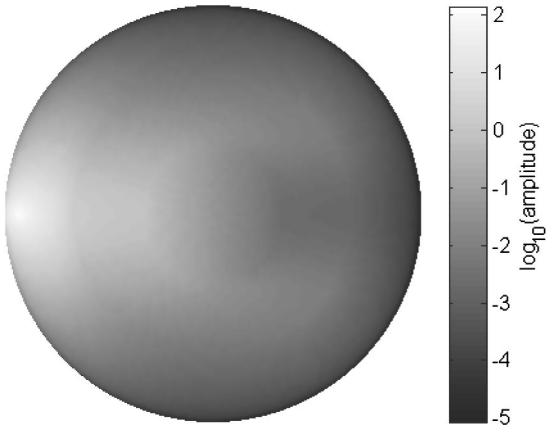

FIG. 5. Internal amplitude field calculated using the FEM.

by the boundary conditions (39). Hence, we see that Φ_{av} must satisfy

$$-\nabla_\perp \cdot \mathsf{D}_\perp \nabla_\perp \Phi_{\mathrm{av}} + \left(\mu_a - \frac{i\omega}{c}\right)\Phi_{\mathrm{av}} = Q_{0,\mathrm{av}}$$

in U, where $Q_{0,\mathrm{av}} = Q_{0,\mathrm{av}}(x,y)$ is the averaged source

$$Q_{0,\mathrm{av}}(x,y) = \int_{-\infty}^{\infty} Q_0(x,y,z)dz.$$

In particular, if the original source is a point source at $(x,y,z) = (x_0,y_0,h)$, i.e., $Q_0 = Q_0(\omega)\delta(x-x_0)\delta(y-y_0)\delta(z-h)$ we have $Q_{0,\mathrm{av}}(x,y) = Q_0(\omega)\delta(x-x_0)\delta(y-y_0)$, i.e., the source $Q_{0,\mathrm{av}}$ is a point source in the 2D model as well. To make the 2D boundary data compatible with the 3D data, we need to integrate the boundary data along the cylinder. In particular, if we model the 3D data collection by vertical line detectors, they correspond to 2D point detectors.

E. Results

Figures 3 and 4 show the results calculated with Monte Carlo (MC) simulation (10^9 photons), the FEM, and the BEM. Figure 3 plots the amplitude (using a logarithmic scale) and Fig. 4 the phase angle of the complex photon

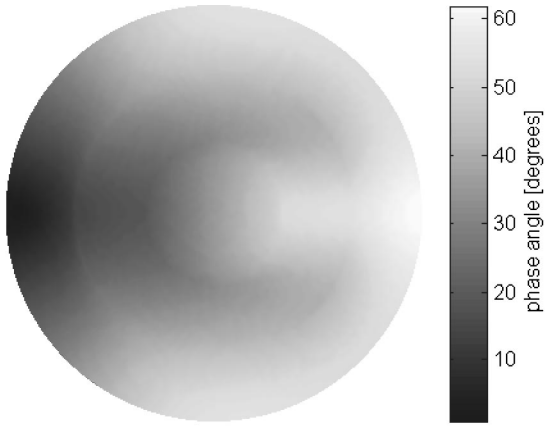

FIG. 6. Internal phase angle field calculated using the FEM.

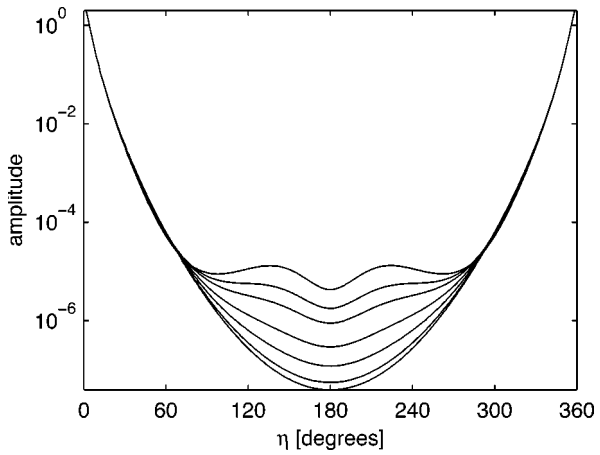

FIG. 7. The logarithm of the amplitude on the boundary calculated with the FEM using different values of the anisotropy fraction *f*. From top to bottom, the curves were calculated using $f=0.9$, 0.8, 0.7, 0.5, 0.3, 0.1, and 0, corresponding to the isotropic case.

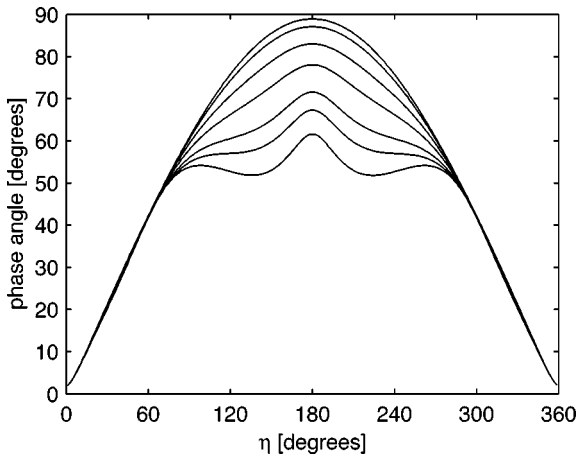

FIG. 8. The phase angle on the boundary calculated with the FEM using different values of the anisotropy fraction *f*. From bottom to top, the curves were calculated using $f=0.9$, 0.8, 0.7, 0.5, 0.3, 0.1, and 0, corresponding to the isotropic case.

density measured on the boundary. Because of the different source models and intensities, the amplitude was scaled for the MC and BEM curves using the FEM/MC and FEM/BEM ratios, respectively, calculated at the boundary position angle $\eta=45°$, as the scaling factors. Figures 5 and 6 show internal maps of the same quantities. Figure 5 plots the internal amplitude field and Fig. 6 the internal phase field of the body calculated using the FEM.

To demonstrate the effect of the strength of the anisotropy on data, the FEM calculation was performed using different values for the fraction *f* in the anisotropic region. Figures 7 and 8 demonstrate the effect of varying *f* on boundary data.

IV. CONCLUSIONS

In this paper we have proposed a model for anisotropic scattering that can be applied using the radiative transfer model. By deriving the diffusion approximation using this scattering model, we obtained the corresponding anisotropic diffusion model and were able to compare the radiative transfer and the diffusion models in the anisotropic case. Numerical examples were calculated using a relatively simple case for the anisotropy. Based on the results, the diffusion model is able to describe the anisotropic behavior relatively well, provided that the anisotropy considered is simple enough to be presented within the diffusion framework.

ACKNOWLEDGMENTS

This work was supported by the Academy of Finland and the Finnish Cultural Foundation. The authors would like to thank Wellcome Trust for a Biomedical Research Collaboration grant. J.H. would like to thank Dr. J. Nenonen, Helsinki University of Technology, for supporting her work.

[1] S.R. Arridge, Inverse Probl. **15**, R41 (1999).
[2] G. Marquez, L.V. Wang, S. Lin, J.A. Schwartzand, and S.L. Thomsen, Appl. Opt. **37**, 798 (1998).
[3] S. Nickell, M. Hermann, M. Essenpreis, T.J. Farrell, U. Krämer, and M.S. Patterson, Phys. Med. Biol. **45**, 2873 (2000).
[4] A. Kienle, F.K. Forster, R. Diebolder, and R. Hibst, Phys. Med. Biol. **48**, N7 (2003).
[5] J. Heino and E. Somersalo, Inverse Probl. **18**, 559 (2002).
[6] L. Dagdug, G.H. Weiss, and A.H. Gandjbakhche, Phys. Med. Biol. **48**, 1361 (2003).
[7] S. Chandrasekhar, *Radiative Transfer* (Oxford University Press, London, 1950).
[8] L.G. Henyey and J.L. Greenstein, Astrophys. J. **93**, 70 (1941).
[9] M. Schweiger, S.R. Arridge, M. Hiraoka, and D.T. Delpy, Med. Phys. **22**, 1779 (1995).
[10] E. Okada, M. Firbank, M. Schweiger, S.R. Arridge, M. Cope, and D.T. Delpy, Appl. Opt. **36**, 21 (1997).
[11] M. Bonnet, *Boundary Integral Equation Methods for Fluids and Solids* (Wiley, Chichester, 1999).
[12] A.A. Becker, *The Boundary Element Method in Engineering. A Complete Course* (McGraw-Hill, London, 1992).
[13] G. Beer, *Programming the Boundary Element Method. An Introduction for Engineers* (Wiley, Chichester, 2001).